Turkish Journal of Electrical Engineering & Computer Sciences

http://journals.tubitak.gov.tr/elektrik/

Research Article

Turk J Elec Eng & Comp Sci
(2013) 21: 1455 – 1464
© TÜBİTAK
doi:10.3906/elk-1012-958

A linearly slotted waveguide antenna and comparison of it with a sinusoidal one

Alp Oral SALMAN*
Electronics and Telecommunication Engineering Department, Faculty of Engineering,
Kocaeli University, Kocaeli, Turkey

Received: 31.12.2010 • **Accepted:** 27.06.2011 • **Published Online:** 12.08.2013 • **Printed:** 06.09.2013

Abstract: A linearly slotted waveguide antenna (LSWA) is investigated. The slot is placed in one of the narrow faces of a rectangular waveguide, which operates at Ka-band (26.5–40 GHz), which is in a frequency range including upper microwaves and the lower edge of millimeter waves. Analytically, the magnetic current approach is applied. Some antenna parameters of this structure are experimentally measured and it is observed that the antenna radiates a single transversal-polarized beam that scans with frequency. The experimentally obtained patterns in 2 perpendicular planes are also correlated with analytical and numerical patterns that use the magnetic current model and HFSS, respectively. Approximate maximum directivity and side lobe level of the antenna are 20 dBi and –10 dB, respectively. In a frequency range of 23–35 GHz, efficiency above 75% is obtained by this investigated antenna. Travelling wave parameters of the antenna are also calculated. The antenna is a fast-wave structure and exhibits frequency-scanning behavior with an average scanning rate of 2.14°/GHz. Some of the results of the investigated LSWA are also compared with the results of the sinusoidal slotted waveguide antenna (SSWA) investigated in a previous study by the author. The directivity and efficiency of the linear slot is better than that of the sinusoidal slot, while the other characteristics are similar. Thus, the LSWA exhibits a better performance than the SSWA does if we consider the transversal E_ϕ polarization (SSWA has another polarization as well, which is longitudinal E_θ polarization). It is also concluded that this frequency-scanning Ka-band LSWA can be used in telecommunications and radar applications.

Key words: Slotted waveguide antennas, linear slot, sinusoidal slot, travelling wave, fast wave radiated structures, leaky wave, Ka-band, millimeter waves

1. Introduction

Although slotted waveguide antennas are one of the oldest antenna types [1], they are still applied in telecommunication and radar systems due to their superiority. The advantages of this type of antenna are their simple and cheap structure, and high efficiency [2]. Polarization purity is another property of slotted waveguide antennas [3]. When a rectangular waveguide is chosen for slotting, both faces (narrow or broad faces) can be preferred. Because the narrow face of a rectangular waveguide has unidirectional surface electric current densities (Figure 1), a linear long slot in this face will be the correct choice for obtaining strong radiation. A linearly slotted waveguide antenna is a leaky-wave structure because electromagnetic power continuously leaks from the slot. At least 90% of input power is required to radiate from the slot [2,3]. The radiation of a slotted waveguide antenna in any form is analytically formulated by the magnetic current approach [4,5]. When the length of the slot is longer than several wavelengths, this radiator can be classified as a travelling wave slot antenna [6]. A travelling wave structure [7] is characterized by its propagation constant.

*Correspondence: oral.salman@kocaeli.edu.tr

There are also some theoretical investigations in the literature involving a narrow slot in a rectangular waveguide [1,8,9]. In those previous studies, the slotted waveguide antennas were mostly investigated to analyze circuital properties and travelling wave parameters. However, in our study, a field pattern analysis of a travelling wave linear slot is done with the application of the magnetic current model for the analytical investigation and additionally the measured and the calculated patterns are correlated with the numerical ones. Thus, there is a chance to show the validity of the magnetic current model and the compatibility of the analytical and numerical patterns with the measured ones.

Another interesting topic that is investigated in this paper is a comparison of the linear slot to another one: a sinusoidal slot, which was investigated in a previous study by the author [10]. In that paper it was shown that the sinusoidal slotted waveguide antenna (SSWA) has 2 beams, which are in 2 different polarizations. Some characteristics of the transversal-polarized beam of the SSWA exhibit similarities with those of the LSWA, which is investigated in this study. The results obtained from this comparison will be discussed in the next sections of the paper. Additionally, the radiation properties and travelling wave parameters of the LSWA such as far-field pattern, directivity, and velocity ratio, will be demonstrated to show the effectiveness of the antenna.

2. The theory

The radiated far-zone fields of a travelling wave linear slot in a narrow face of a rectangular waveguide will be formulated as given in [10]. Formulation starts with definition of a fictitious magnetic current $\vec{I}_m$ in the slot [4,5]. This current is assumed to exist because electric surface current density ($\vec{J}_s$) lines are cut by the slot [2]. The linear slot is shown in Figure 1. The vector lines of magnetic field $\vec{H}$ are perpendicular to the lines of ($\vec{J}_s$).

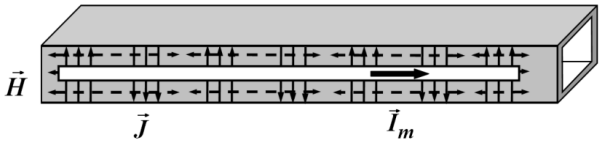

Figure 1. A travelling wave linear slot, where a fictitious magnetic current $\vec{I}_m$ flows along. The solid lines and the dashed lines on the wall refer to the vector lines of electric surface current density ($\vec{J}_s$) and magnetic field ($\vec{H}$), respectively.

The analysis is straight forward and similar to that of the electric current complementary thin wire antennas [11]. The linear slot on the waveguide's narrow wall (Figure 2) has $2z_0$ length, which is at least several wavelengths long ($l > \lambda$) to satisfy the travelling wave condition. It is supposed that the waveguide is properly matched and only a forward current exists in the linear slot. This magnetic current on the point $z = z'$ is given as

$$\vec{I}_m = \hat{a}_z I_m = \hat{a}_z I_{m0} \exp?(-\gamma_z z'), \tag{1}$$

where I_{m0} and γ_z refer here to magnitude of magnetic current and propagation constant of the current wave along the slot, respectively. The propagation constant is represented as $\gamma_z = \alpha_z + j\beta_z$ [11,12], where α_z is the attenuation constant,[1] which is the summation of leakage and conduction losses, in Np/m, and β_z is the phase

[1]When the loss power P_{loss} due to conductivity of metallic waveguide walls is negligible (see Section 3.3 for calculation), α_z contains only the leakage power due to the radiation from the slot. It is also called the "leakage constant" for a leaky-wave structure for this case [2] and is closely related to the leaked or radiated power P_{rad} from the structure. The leakage constant is formulated as $\alpha_z = -(1/2L)\ln(P_L/P_0)$, where L is length of the leaky-wave structure, P_0 is the input power, and P_L is the remaining power at the end of the structure.

constant in rad/m. The exponential term in the equation shows that this current wave is a travelling wave.

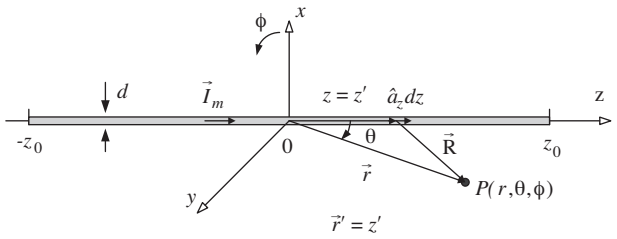

Figure 2. A sketch of a properly matched linear slot to illustrate the calculation of radiated fields arising from a magnetic current $\vec{I}_m$.

Electric vector potential generated by magnetic current $\vec{I}_m$ given in [10] is $\vec{F}(\vec{r}) = (\varepsilon_0/4\pi)\int_{-z_0}^{z_0}\left(\vec{I}_m \exp(-jkR)\Big/R\right).d\vec{z}'$. k is the phase constant of radiated free space wave here. The components of electric vector potential in Cartesian coordinates at point $P(r\theta\phi)$ can be written as

$$F_x(x,y,z) = F_y(x,y,z) = 0$$

$$F_z(x,y,z) = \left(\frac{\varepsilon_0 I_{m0}}{4\pi}\right)\int_{-z_0}^{z_0}\exp(-\gamma_z z')\frac{\exp(-jkR)}{R}.dz'$$

These components above are transformed to spherical components using an appropriate transformation matrix [11]. Thus, the spherical components of electric vector potential are obtained as

$$F_r = F_z cos\theta$$

$$F_\theta = -F_z sin\theta$$

$$F_\phi = 0$$

Finally, far field electric fields radiated by a linear slot can be written as follows:

$$\vec{E}(r,\theta,\phi) = j\omega\eta_0\hat{a}_r \times \vec{F}(r,\theta,\phi) = \begin{cases} E_r \cong 0 \\ E_\theta \cong -j\omega\eta_0 F_\phi \\ E_\phi \cong -j\omega\eta_0 F_\theta \end{cases} = 0, \quad (2)$$

where $\hat{a}_r$ and η_0 refer to unit vector of r component and wave impedance of free space $(= 120\pi)$, respectively.

3. Measurements

3.1. Antenna pattern measurements of linear slot and correlation with calculated and numerical ones

For measurements, a linearly slotted waveguide antenna (LSWA) was created using a CNC milling machine. A rectangular Ka-band (26.5–40 GHz) waveguide was chosen for slotting and a linear slot was milled in a narrow face of this waveguide (Figure 3). According to IEEE, the Ka-band is the uppermost part of the microwave region. However, the RF band's designation informs us that this range also takes part in the EHF band, which is at the lower edge of the millimeter wave region starting from 30 GHz. The dimensions of the slot are 1 mm in width and 80 mm in length, which equal $\lambda/10$ and 8λ at 30 GHz, respectively. Thus, the slot is thin enough to obtain a linear magnetic current and long enough to get travelling waves along the slot. It is seen in Figure 3 that the antenna is properly matched with a 50-Ω coaxial-type broad band load.

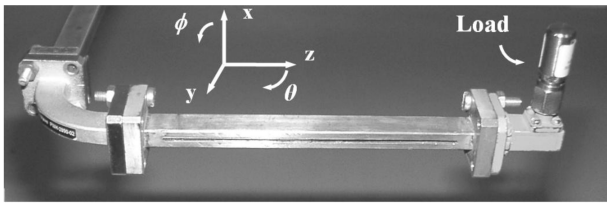

Figure 3. Photo of the created linearly slotted waveguide antenna (LSWA).

The far-field pattern measurements were performed in 2 major perpendicular planes: $y-z$ and $x-y$ planes (see Figure 3). For the $y-z$ plane measurement, $\phi=\pi/2$ and there is no change in the electric vector potential components given in Eq. (3) because none of the components depend on the coordinate ϕ. However, for the $x-y$ plane measurement $\theta=\pi/2$ and these components become $F_\theta=-F_z$ and $F_r=-F_\phi=0$. After obtaining electric vector potential components, the radiated far-zone electric fields are calculated for 2 major planes using Eq. (2).

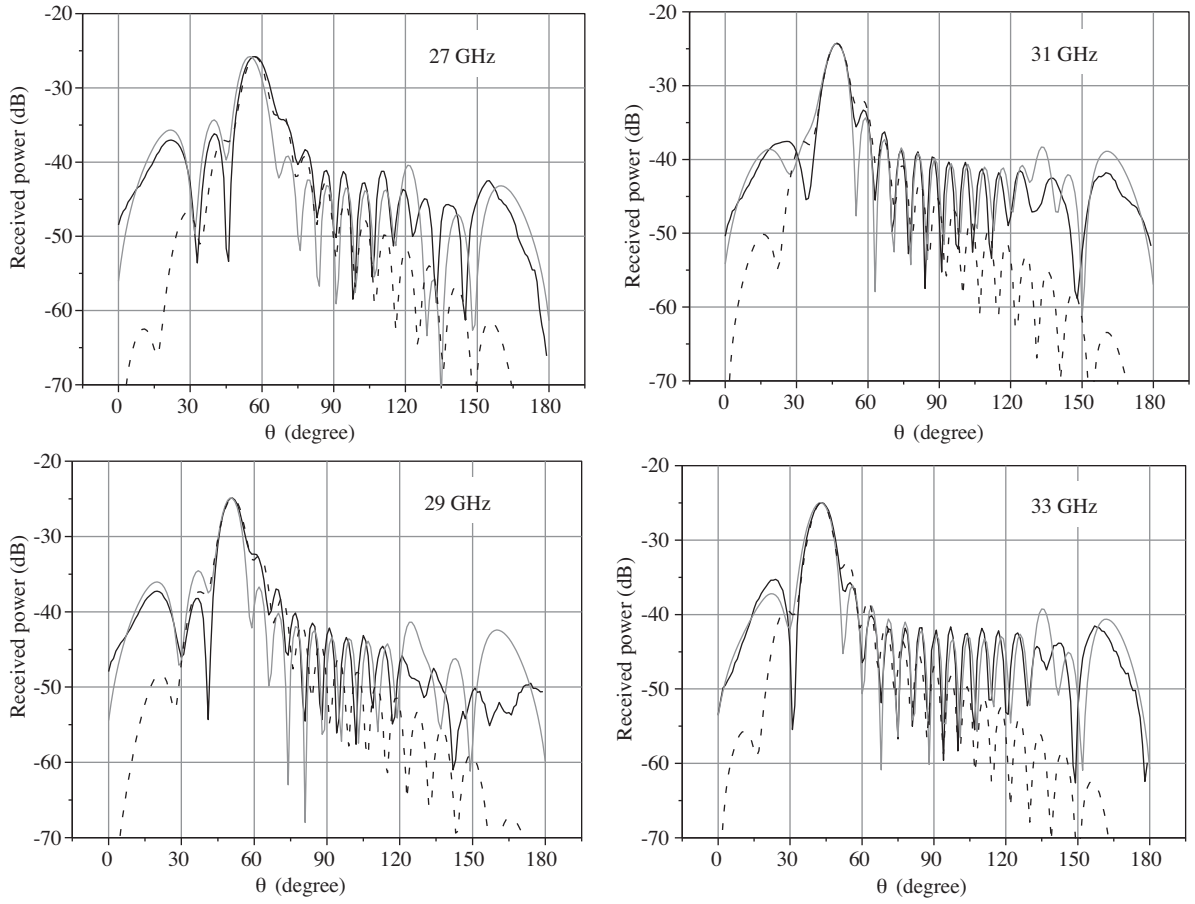

Figure 4. The measured (——), calculated (— — —), and numerical (by HFSS) (——) far-field E_ϕ patterns of the LSWA in the $y-z$ plane for 4 different frequencies.

In the measurements, the far-field patterns of the antenna were obtained at the Ka-band (26.5–40 GHz) using a system including an Agilent N5230A vector network analyzer (VNA). The measured far-field patterns were in the $y-z$ and $x-y$ planes as formulated above. In Figure 4, measured, calculated, and numerical

far-field E_ϕ patterns of the LSWA in the $y-z$ plane for 4 different frequencies are given. While the simulation package program HFSS was used for obtaining the numerical patterns, the calculated ones were created by a MATLAB code using the analytical magnetic current model formulated in Section 2.

An analysis of the patterns in Figure 4 gives us the following results. Although the numerical and calculated field patterns match with the measured ones perfectly for the main lobe, the calculated patterns give a better match with the measured ones for the shoulder at the right-hand side of the main lobe, which is around –10 dB. However, the numerical patterns match the measured ones better than the calculated ones for the remaining part of the pattern at the side lobes, which is below –10 dB. On the other hand, the calculated patterns start to diverge from the measured and numerical patterns below –20 dB.

In Figure 5, the measured and calculated $x-y$ plane normalized far-field E_ϕ patterns of the LSWA at 27 GHz can be seen and compared with the corresponding $y-z$ plane far-field pattern of the same component given in Figure 4. According to the figures, the $x-y$ plane pattern is wider than the $y-z$ plane pattern because the aperture of the antenna is smaller in the $x-y$ plane than in the $y-z$ plane. It can be concluded that the LSWA has a fan-shaped pattern.

For the full frequency range, the measured $y-z$ plane E_ϕ field peak power level varying with frequency for the LSWA obtained from Figure 4 is shown in Figure 6 (peak power levels of the SSWA are also included for comparison). It can be observed that the peak power level of the LSWA varies in a 2-dB interval in the measurement frequency range and the maximum power level is obtained at 31 GHz.

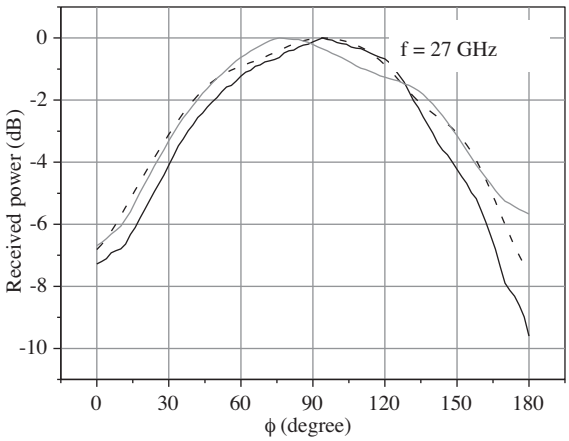

Figure 5. The measured (——), calculated (— — —), and numerical (by HFSS) (——) normalized far-field E_ϕ patterns of the LSWA in the $x-y$ plane at 27 GHz.

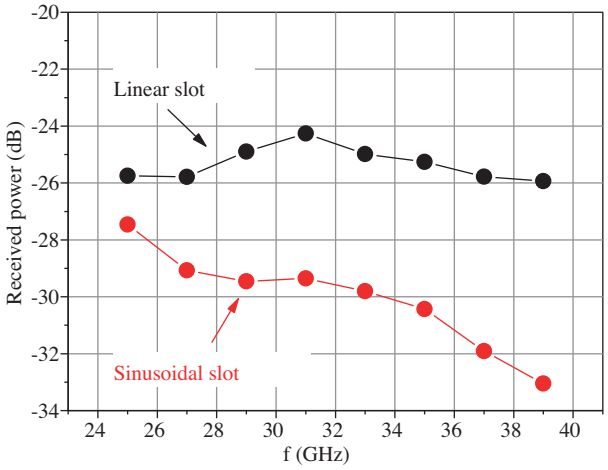

Figure 6. The measured peak power levels of E_ϕ beam in the $y-z$ plane for the LSWA and SSWA. The result of SSWA given here is after [10].

3.2. Other radiation and travelling wave parameters of the LSWA and comparison to those of the SSWA

In this section, the remaining radiation parameters and travelling wave parameters of the LSWA will be investigated. Some of the results will also be compared to the E_ϕ beam results of the SSWA[2] [10], which

[2]The author has also published other kinds of travelling wave sinusoidal-shaped antenna and resonator structures, i.e. sinusoidal wire antennas [13,14] and resonator [15,16] and sinusoidal strip-microstrip antennas [17]. The radiated fields of these antennas are calculated by the electric current model [11] as a common property. In addition, 2 studies related to a dielectric leaky-wave antenna excited by sinusoidal metallic gratings were also published [18,19].

can be seen in Figure 7. The SSWA has 2 field components, transversal E_ϕ and longitudinal E_θ. However, the LSWA has only one component, E_ϕ, due to its one-dimensional geometry. The corresponding field component of the SSWA is the E_ϕ component, which is used for the comparison to the same field component of the LSWA. The SSWA was created before using a CNC milling machine for a previous study [10] and all results related to the SSWA, which are used in this paper for comparison purposes, were obtained in that study. A SSWA can be characterized by its period (Λ), amplitude (L_0), and the number of periods (N), and these values were chosen as $\Lambda = 7$ mm, $L_0 = 1.5$ mm, and $N = 12$, respectively. Therefore, the total length of the sinusoidal slot was $\Lambda \times N = 84$ mm, which is approximately the same length as the linear slot (80 mm). One can compare the far-field patterns of this antenna given in [10], which are not presented here due to the lack of space, to the patterns of the LSWA given in Figures 4 and 5.

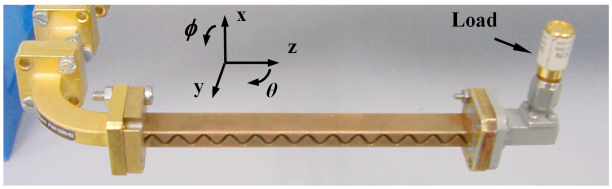

Figure 7. The SSWA, which was investigated in [10]. See the text for the dimensions of the antenna. Some characteristics of its transversal component (E_ϕ) are compared to those of the LSWA, which is investigated in this paper.

The measured peak power levels of the E_ϕ component of the SSWA are given in Figure 6 for comparison with those of the LSWA. It is obvious that the efficiency of the LSWA is on average 4–5 dB better than that of the SSWA. This efficiency difference increases with frequency.

Figure 8 shows the measured beam pointing angle for the $y-z$ plane measurement and the calculated velocity ratio υ_p/c (the ratio of the phase velocity, which propagates along the slot to the light speed) variations versus frequency for the LSWA and SSWA. The beam pointing angle is the angle where the maximum radiation locates in θ-coordinate (check field patterns given in Figure 4). The velocity ratio is also related to the phase constants with the relation $\upsilon_p/c = k/\beta_z$. The solid lines in the figure are the best-fitted lines through the points. A nonlinear decaying behavior with frequency can be seen from the figure for the beam angle and the calculated velocity ratios. The beam angle (see Figure 8 (a)) varies 30° in a 14-GHz frequency range (25–39 GHz), giving an average scanning rate of 2.14°/GHz for the LSWA. The average scanning rate of the E_ϕ beam of the SSWA was found in [10] as 1.93°/GHz, which is slightly lower than the value of the LSWA. The υ_p/c values in Figure 8(b) are obtained by matching the calculated patterns with the measured ones. υ_p/c is higher than unity; thus the structure is a fast wave structure, which is a natural outcome of the slotted waveguide structures [8]. It can be seen that the velocity ratio of the sinusoidal slot is less than that of the linear slot. Thus, the wave propagates slower in the sinusoidal slot than in the linear slot and the difference in the velocity ratios becomes less at the higher frequency part of the operating frequency band. It is expected because the electrical length of the sinusoidal slot is greater than the length of the linear slot that the wave propagates slower along the sinusoidal slot.

The half-power beam widths (HPBWs) in the 2 major measurement planes ($y-z$ and $x-y$ planes) and the calculated antenna directivity, which is $D \cong 41,253/(\Theta_1\Theta_2)$, where Θ_1 and Θ_2 are the HPBWs in the 2 major planes ($y-z$ and $x-y$ planes) in degrees [11], versus frequency for the LSWA and SSWA are shown in Figure 9. For the LSWA, it is observed from Figure 9(a) that the beam measured in the $x-y$ plane is wider

than the beam in the $y-z$ plane, which is consistent with the results obtained from the field patterns given in Figures 4 and 5. The beam in both planes ($y-z$ and $x-y$ planes) becomes narrower with the increasing frequency (high frequency narrowing). The directivity values (see Figure 9(b)) for the linear slot increases from 15 dBi to 20 dBi in the frequency range 27–33 GHz. The HPBW value of the sinusoidal slot in the $y-z$ plane is quite similar to that of the linear slot. The $y-z$ plane beam of the linear slot is on average 1.5° narrower than that of the sinusoidal slot. However, for the $x-y$ plane, the HPBWs of the beams are different. The directivities calculated from the HPBWs of both antennas vary for this reason and the directivity of the linear slot is approximately 15% larger than that of the sinusoidal slot.

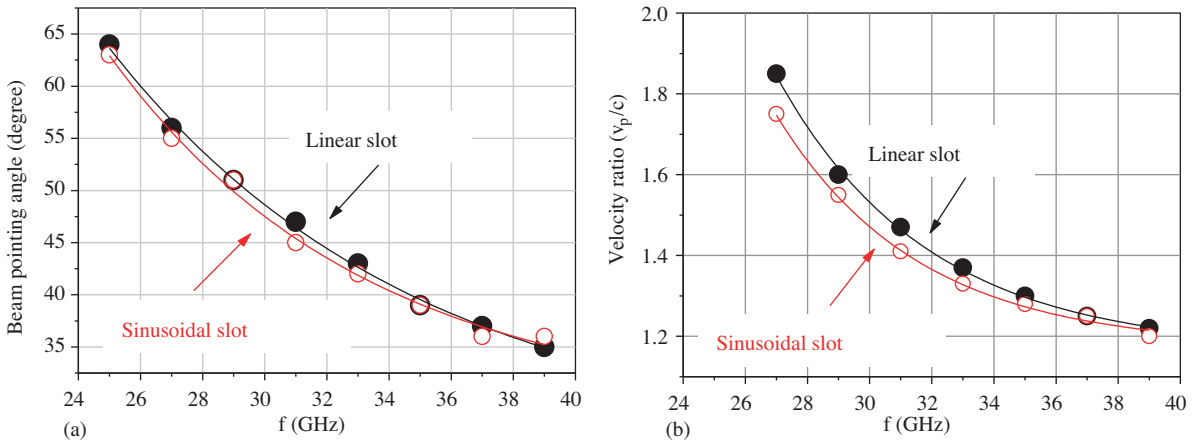

Figure 8. (a) The measured beam pointing angle of the E_ϕ field for the $y-z$ plane measurement and (b) the calculated velocity ratio v_p/c variations versus frequency for the LSWA (–●–) and SSWA (–○–). The solid lines are the best-fitted lines through the points. The results of the SSWA are after [10].

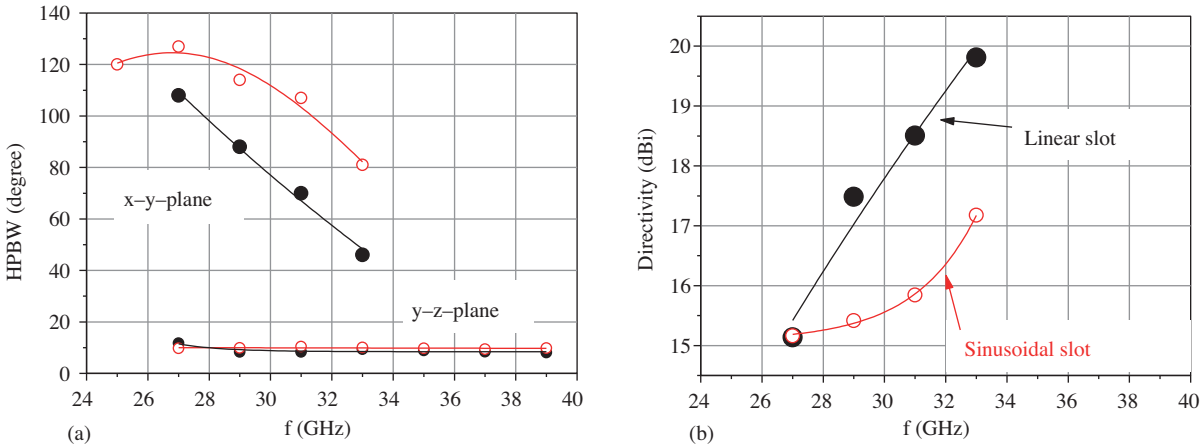

Figure 9. (a) The HPBWs in the 2 major measurement planes and (b) the calculated antenna directivities of the LSWA (–●–) and SSWA (–○–). The results of the SSWA are after [10].

3.3. S-parameters measurement and antenna efficiency of the LSWA and comparison to those of the SSWA

In the experiment, S-parameters (S_{11} and S_{21}) were additionally measured using an Agilent N5230A VNA. The calibration steps of the VNA for slotted waveguide antennas are as follows. First, the slotted waveguide part of

the LSWA was disassembled and the broad-band 50-Ω load was disconnected from the n-type waveguide–coaxial cable transition on the right connected to the flange of waveguide on the left (see Figure 7 for their positions). Then the VNA was fully calibrated. Finally, the slotted part of the antenna was reassembled and the VNA became ready to measure S-parameters. During S_{11} measurements, the broad-band 50-Ω load was additionally connected to the antenna. In Figure 10, the measured S-parameters (S_{11} and S_{21}) of the LSWA are shown.

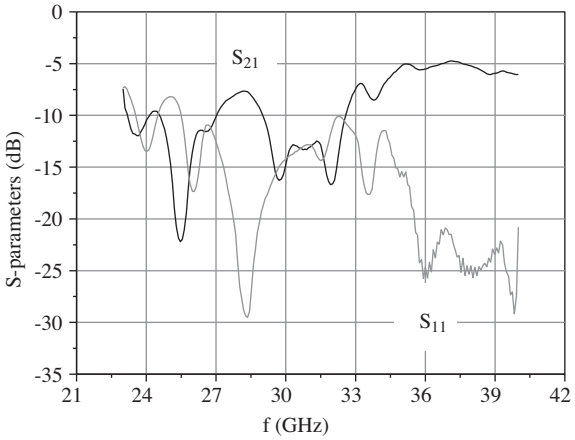

Figure 10. Measured S-parameters (S_{11} and S_{21}) of the LSWA.

Using measured S-parameters, the antenna efficiency e can easily be calculated. The calculation method is as described in [10]. Briefly, if we assume that the radiating antenna is a 2-port network (see Figure 11), we may write the power equation of this network as $P_{in} = P_r + P_t + P_{rad} + P_{loss}$. In this power equation, P_{in} is the input power supplied to the antenna, P_r is the reflected power from port 1 of the antenna network due to the mismatch, P_t is the transmitted power from port 1 to port 2, P_{rad} is the radiated power from the antenna, and P_{loss} is the lost power due to the finite conductivity of the waveguide walls. According to the definition of S-parameters, $P_r = |S_{11}|^2 P_{in}$ and $P_t = |S_{21}|^2 P_{in}$, where S_{11} and S_{21} are measured S-parameters. Note that S-parameters have to be converted from dB to linear scale in equations. The calibration makes P_{in} unity ($P_{in} = 1$). Because for an 80 mm long standard Ka-band waveguide, the lost power that is dissipated in the metallic waveguide walls is calculated around 0.05 dB [12], the lost power is negligible for the LSWA ($P_{loss} \cong$). Thus, we obtain radiated power P_{rad} as

$$P_{rad} = 1 - \left\{ |S_{11}|^2 + |S_{21}|^2 \right\}. \tag{3}$$

Finally, the antenna efficiency e in percentage is found in terms of the radiated power P_{rad},

$$e = \frac{P_{rad}}{P_{in}} \times 100 = 100 P_{rad}. \tag{4}$$

The antenna efficiency of the LSWA and SSWA, which is calculated using (4), is given in Figure 12. For the linear slot, the maximum efficiency achieved is 95% and the efficiency is over 75% in the frequency range 23–34 GHz, showing that the antenna efficiency is less at the high frequency region of the band. Additionally, the linear slot has higher efficiency on average and the efficiency of the sinusoidal slot drops fast after 27 GHz. This result is consistent with the peak power levels observed in Figure 6. One can conclude that the LSWA is a more efficient and broadband antenna compared to the SSWA.

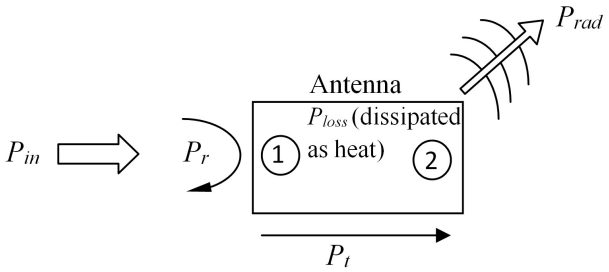

Figure 11. Two-port antenna network.

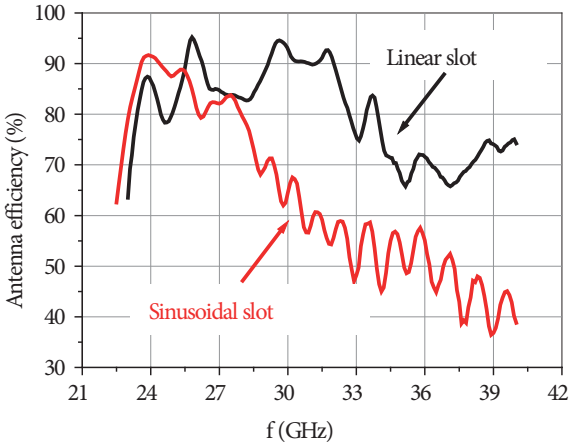

Figure 12. Calculated antenna efficiency in percentage for the LSWA and SSWA. The result of the SSWA is after [10].

4. Summary and conclusion

The travelling wave LSWA was investigated by this study in the lower edge of the millimeter-wave region at the Ka-band. Some results were also compared with those of the transversal field component ($E_{\emptyset}$) of the SSWA, which was investigated in a previous study [10]. The magnetic current model is used for the analytical approach. The measured far-field patterns are correlated with the calculated and numerical ones. According to the calculated velocity ratios (v_p/c), the LSWA is a fast wave structure as expected for a slotted waveguide antenna. The antenna has 20-dBi directivity at maximum and the beam frequency scanning interval is 30° in a 14-GHz frequency range, giving an average scanning rate of 2.14°/GHz, which is very close to the rate of the SSWA (1.93°/GHz) [10]. It is observed from the measured field patterns that the beam measured in the $x-y$ plane is wider than the beam measured in the $y-z$ plane beam because the antenna has a smaller antenna aperture in the $x-y$ plane.

Nonlinear decaying behaviors are observed for the frequency variations of the beam angle and velocity ratio. We observed that the beam angle and velocity ratio of SSWA are slightly smaller than those of the LSWA at a fixed frequency. While the HPBW values in the $y-z$ plane of the LSWA and SSWA are quite close, in the $x-y$ plane they differ. It causes a change in directivity values, where the directivity of the SSWA is 15% smaller.

The antenna efficiency variation with the frequency was also calculated using S-parameter measurements and a maximum of 95% efficiency was achieved, while the efficiency was over 75% in the frequency range 23–34 GHz. The SSWA exhibits less antenna efficiency than LSWA. The results show that the linear slot has better antenna characteristics compared to the SSWA. This situation can be explained in the following manner. The SSWA has 2 field components, transversal E_{ϕ} and longitudinal E_{θ}, due to its geometry. However, the LSWA has a single field component, transversal E_{ϕ}. Thus, the electromagnetic power is shared in 2 field components for the sinusoidal slot. This can cause a decrease in peak power levels of each field component and in the efficiency of the sinusoidal slot.

It is concluded that the LSWA investigated in this study can be used in radar or any telecommunication applications and exhibits better performance than the SSWA if we consider only the transversal polarization E_{ϕ}.

Acknowledgment

The author would like to thank Harun Çetinkaya for his contributions in the simulations of the antenna.

References

[1] A.F. Stevenson, "Theory of slots in rectangular wave-guides", Journal of Applied Physics, Vol. 19, pp. 24 – 38, 1948.

[2] R.C. Johnson, Antenna Engineering Handbook, 4rd ed., McGraw-Hill, Inc., New York, 1993.

[3] J.L. Volakis, Antenna Engineering Handbook, 3rd ed., McGraw-Hill, Inc., New York, 2007.

[4] E.C. Jordan, Electromagnetic Waves and Radiating Systems, Prentice-Hall, New Delhi, 1967.

[5] E.A. Wolf, Antenna Analysis, John Wiley & Sons, Inc., New York, 1966.

[6] J.N. Hines, V.H. Rumsey, C.H. Walter, Traveling-wave slot antennas, Proc. IRE, Vol. 41, pp. 1624–1631, 1953.

[7] C.H. Walter, Traveling Wave Antennas, McGraw Hill Co., New York, 1965.

[8] L.O. Goldstone, A.A. Oliner, "Leaky-wave antennas I: Rectangular waveguides", IRE Trans. on Ant. Prop., Vol. 7, pp. 307–319, 1959.

[9] A.A. Oliner, "The impedance properties of narrow radiating slots in the broad face of rectangular waveguide: Part I and II", IRE Trans. on. Ant. Prop., Vol. 5, pp. 4–20, 1957.

[10] A.O. Salman, "Millimeter-wave antenna of a travelling wave long sinusoidal slot in the narrow face of a rectangular waveguide", Journal of Infrared, Millimeter, and Terahertz Waves, Vol. 31, pp. 1438–1451, 2010.

[11] C.A. Balanis, Antenna Theory Analysis and Design, 3rd ed., Wiley, New Jersey, Canada, 2005.

[12] C.A. Balanis, Advanced Engineering Electromagnetics, Ch. 2, John Wiley & Sons Inc., 1989.

[13] A.O. Salman, D. Dibekci, S. Gavrilov, A. Alexei Vertiy, "The millimeter wave radiation of a traveling wave sinusoidal wire antenna", International Journal of Infrared and Millimeter Waves, Vol. 29, pp. 465–485, 2008.

[14] A.O. Salman, D. Dibekci, S.P. Gavrilov, A. Alexei Vertiy, "The radiation properties of a novel wire antenna for the security fence radar", IEEE Transactions on Antennas and Propagation, Vol. 56, pp. 2852–2864, 2008.

[15] A.O. Salman, "Phase velocity measurement of surface wave propagating along a goubau-line: wire resonator method", IEEE EUROCON 2009, St Petersburg, Russia, 2009.

[16] A.O. Salman, "Phase velocity measurement using a sinusoidal wire resonator", Microwave Optical and Technology Letters, Vol. 2, pp. 103–107, 2010.

[17] A.O. Salman, H. Cetinkaya, A.A. Vertiy, "Actively and passively-excited sinusoidal microstrip and PCB strip antennas operating at K and millimeter-wave bands", Microwave Optical and Technology Letters, Vol. 50, pp. 1302–1308, 2008.

[18] A.O. Salman, "The millimeter wave radiation of a dielectric leaky-wave antenna coupled with a diffraction grating: broad-face interaction", Journal of Infrared, Millimeter, and Terahertz Waves, Vol. 31, pp. 196–213, 2010.

[19] A.O. Salman, "The millimeter wave radiation of a dielectric leaky-wave antenna coupled with a diffraction grating for the broadside radiation: Narrow-face interaction", Journal of Infrared, Millimeter, and Terahertz Waves, Vol. 31, pp. 1032–1047, 2010.